

Improved analysis of the $(\mathcal{O}_7, \mathcal{O}_7)$ contribution to $\bar{B} \rightarrow X_s \gamma \gamma$ at $\mathcal{O}(\alpha_s)$ H. M. Asatrian,^{1,*} C. Greub,^{2,†} and A. Kokulu^{3,‡}¹*Yerevan Physics Institute, 0036 Yerevan, Armenia*²*Albert Einstein Center for Fundamental Physics, Institute for Theoretical Physics, University of Bern, CH-3012 Bern, Switzerland*³*Department of Mathematical Sciences, University of Liverpool, L69 7ZL Liverpool, United Kingdom*
(Received 9 December 2016; published 16 March 2017)

The present study is devoted for an improved analysis of the self-interference contribution of the electromagnetic dipole operator \mathcal{O}_7 to the double differential decay width $d\Gamma/(ds_1 ds_2)$ for the inclusive $\bar{B} \rightarrow X_s \gamma \gamma$ process, where the kinematical variables s_1 and s_2 are defined as $s_i = (p_b - q_i)^2/m_b^2$ with p_b, q_1, q_2 being the momenta of the b -quark and two photons. This calculation completes the next-to-leading-logarithmic (NLL) QCD prediction of the numerically important self-interference contribution of \mathcal{O}_7 by keeping the full dependence on the strange-quark mass m_s , which is introduced to control possible collinear configurations of one of the photons with the strange quark. Our results are given for exact m_s , in contrast to an earlier work where only logarithmic and constant terms in m_s were retained. This improved NLL result for the $(\mathcal{O}_7, \mathcal{O}_7)$ -interference contribution shows that finite m_s effects are only sizable near the kinematical endpoints of the spectrum $d\Gamma/(ds_1 ds_2)$. At the level of the branching ratio, in the phase-space region considered in this paper, it is observed that $\text{Br}[\bar{B} \rightarrow X_s \gamma \gamma]$ does not develop a sizable m_s dependence: the impact on this branching ratio is less than 5% when m_s is varied between 400–600 MeV. For the same phase-space region finite strange quark mass effects for the branching ratio are less than 7%.

DOI: 10.1103/PhysRevD.95.053006

I. INTRODUCTION

In the standard model (SM), flavor changing neutral current transitions [such as $b \rightarrow s \gamma(\gamma)$] are suppressed since they are loop-induced. When going beyond the SM, such processes could provide a unique source for probing physics indirectly at the TeV scale. For instance, in the two-Higgs-doublet-model (2HDM) of type II the inclusive singly radiative decay $\bar{B} \rightarrow X_s \gamma$ is known to have provided a very stringent (almost $\tan\beta$ -independent) lower bound on the charged Higgs boson mass to be $m_{H^\pm} > 480$ GeV at 95% CL. This limit has been obtained by comparing the recent experimental data for $\text{Br}[\bar{B} \rightarrow X_s \gamma]$ with the corresponding theoretical 2HDM results, which are based on the next-to-next-to-leading-logarithmic (NNLL) SM results [1], as well as on the NLL [2–4] and NNLL [5] charged Higgs contributions to the various Wilson coefficients.

Although the branching ratio for the singly radiative decay $\bar{B} \rightarrow X_s \gamma$ is much larger, the double radiative decay $\bar{B} \rightarrow X_s \gamma \gamma$ possesses certain advantages. In contrast to the singly radiative decay, the current-current operators $\mathcal{O}_{1,2}$ contribute to the double radiative decay at order α_s^0 precision (through one-particle irreducible one-loop diagrams), leading to an interesting interference pattern with the contributions associated with the electromagnetic dipole operator \mathcal{O}_7 already at LL precision. As a result,

potential new physics should be clearly visible not only in the total branching ratio, but also in the differential distributions.

The process $\bar{B} \rightarrow X_s \gamma \gamma$ is of direct interest to the new Belle II experiment (SuperKEKB) in Japan, which aims to detect branching ratios as small as 10^{-8} or smaller and will start taking B data in 2018 [6,7]. This calls for more precise SM calculations of this observable. The status of the related works can be summarized as follows: The SM estimates of the branching ratios for $\bar{B} \rightarrow X_s \gamma$ [1,8] and $\bar{B} \rightarrow X_s \ell^+ \ell^-$ are now available even to NNLL precision (see e.g. [9,10] for reviews). Regarding the $\bar{B} \rightarrow X_s \gamma \gamma$ decay, the leading logarithmic (LL) prediction for the branching ratio was known since a long time [11–14], while the first attempts toward a NLL calculation were only made years later by us [15,16], in which the QCD corrections to the numerically dominant $(\mathcal{O}_7, \mathcal{O}_7)$ contribution were worked out in certain approximations which will be detailed in the next paragraph. In 2015, we also provided the contributions stemming from the self-interference of chromomagnetic dipole operator \mathcal{O}_8 [17].

In Ref. [15] we calculated order α_s corrections based on the operator \mathcal{O}_7 to the double differential decay width $d\Gamma/(ds_1 ds_2)$, by taking into account only the leading power terms in s_3 in the underlying triple differential decay width $d\Gamma/(ds_1 ds_2 ds_3)$, where s_3 is the normalized invariant mass squared of the hadronic particles in the final state. In Ref. [16], we worked out the double differential decay width based on the triple differential width, retaining

*hrachia@itp.unibe.ch

†greub@itp.unibe.ch

‡akokulu@liverpool.ac.uk

all powers with respect to s_3 . In that work we approximated, however, the dependence on the strange quark mass m_s , by only keeping logarithmic terms in m_s and the terms which are independent of m_s . As m_s is interpreted as a constituent mass in our setup, varying in a range between 400 and 600 MeV, this approximation is somewhat questionable. In the present work, we therefore give NLL results which take into account the full m_s dependence. We denote these results as *exact results* and the results of Ref. [16] as *results in the limit $m_s \rightarrow 0$* .

We should mention that this inclusive process has also been analyzed in some new physics scenarios [12,14,18]. Also, spectator quark and long distance (resonant) effects were studied in the literature (see e.g. [19–21], [13] and references therein). Further, there have also been several studies on the corresponding exclusive channels $B_s \rightarrow \gamma\gamma$ and $B \rightarrow K\gamma\gamma$, both within [13,19,20,22–28] and beyond the SM [18,20,25,29–37].

Our paper is structured as follows. In Sec. II we discuss the theoretical framework and some preliminaries for the calculations. In Sec. III we work out the double differential distribution $d\Gamma_{77}/(ds_1 ds_2)$ in leading order, i.e., without taking into account QCD corrections to the matrix element

$\langle s\gamma\gamma|\mathcal{O}_7|b\rangle$. In this section we also give the order α_s^0 results when including the effects of the operators \mathcal{O}_1 and \mathcal{O}_2 , keeping the full dependence on m_s .

In Sec. IV we calculate virtual and bremsstrahlung QCD corrections to the double differential decay width $d\Gamma_{77}[\bar{B} \rightarrow X_s\gamma\gamma]/(ds_1 ds_2)$ associated with the operator \mathcal{O}_7 , keeping the full dependence on the strange-quark mass m_s . In Sec. V we give numerical illustrations of our results. In Sec. VI we give a brief summary of our findings.

II. THEORETICAL FRAMEWORK AND KINEMATICAL CUTS

We begin our calculation by identifying the effective Hamiltonian governing $b \rightarrow s\gamma(\gamma)$ transition, after integrating out the heavy degrees of freedom in the SM. This Hamiltonian reads

$$\mathcal{H}_{\text{eff}} = -\frac{4G_F}{\sqrt{2}} V_{ts}^* V_{tb} \sum_{i=1}^8 C_i(\mu) \mathcal{O}_i(\mu), \quad (1)$$

where the operators are defined according to [38] as:

$$\begin{aligned} \mathcal{O}_1 &= (\bar{s}_L \gamma_\mu T^a c_L)(\bar{c}_L \gamma^\mu T_a b_L), & \mathcal{O}_2 &= (\bar{s}_L \gamma_\mu c_L)(\bar{c}_L \gamma^\mu b_L), \\ \mathcal{O}_3 &= (\bar{s}_L \gamma_\mu b_L) \sum_q (\bar{q} \gamma^\mu q), & \mathcal{O}_4 &= (\bar{s}_L \gamma_\mu T^a b_L) \sum_q (\bar{q} \gamma^\mu T_a q), \\ \mathcal{O}_5 &= (\bar{s}_L \gamma_\mu \gamma_\nu \gamma_\rho b_L) \sum_q (\bar{q} \gamma^\mu \gamma^\nu \gamma^\rho q), & \mathcal{O}_6 &= (\bar{s}_L \gamma_\mu \gamma_\nu \gamma_\rho T^a b_L) \sum_q (\bar{q} \gamma^\mu \gamma^\nu \gamma^\rho T_a q), \\ \mathcal{O}_7 &= \frac{e}{16\pi^2} [\bar{s} \sigma^{\mu\nu} (\bar{m}_b(\mu) R + \bar{m}_s(\mu) L) F_{\mu\nu} b], & \mathcal{O}_8 &= \frac{g_s}{16\pi^2} [\bar{s} \sigma^{\mu\nu} (\bar{m}_b(\mu) R + \bar{m}_s(\mu) L) T^a G_{\mu\nu}^a b]. \end{aligned} \quad (2)$$

In Eq. (2), T^a ($a = 1, 8$) are the $SU(3)$ color generators, e and g_s are the electromagnetic and the strong couplings, and $\bar{m}_s(\mu)$ and $\bar{m}_b(\mu)$ are the running s and b -quark masses defined in the $\overline{\text{MS}}$ -scheme. Note that we keep the term involving m_s in the operator \mathcal{O}_7 , as we keep the full dependence on m_s in our work. Further, Eq. (1) takes this compact form only after neglecting the small $V_{ub} V_{us}^*$ element (as $V_{ub} V_{us}^* \ll V_{tb} V_{ts}^*$) and exploiting the unitarity of the unitarity of Cabibbo–Kobayashi–Maskawa (CKM) matrix.

In the effective theory framework, the calculation for the branching ratio (or for a specific differential distribution) can be divided into two parts. The first one deals with perturbative matching calculations of the Wilson coefficients $C_i(\mu)$ appearing in Eq. (1) at the large scale ($\mu \sim m_W$), followed by solving the renormalization-group-equations (RGE) for these coefficients¹ to obtain

¹Solving RGEs requires computing anomalous-dimension-matrices (ADM) of the effective operators to the desired order (see e.g. Refs. [39–41] for the impressive three and four-loop ADM contributions).

their values at the decay scale ($\mu \sim m_b$). The second part consists of calculating the matrix elements of the operators in Eq. (2). At the bottom scale, the strong coupling is still small enough ($\alpha_s(m_b) \sim 0.22$) such that perturbative calculations of the matrix elements are possible.

For the process of interest, the Wilson coefficients at the low scale $C_i(\mu \sim m_b)$ are available today even to NNLO precision (see e.g. the reviews [9,10] and references therein). On the other hand, the matrix elements $\langle s\gamma\gamma|\mathcal{O}_i|b\rangle$ and $\langle s\gamma\gamma\gamma|\mathcal{O}_i|b\rangle$, which in a NLL calculation are needed to order g_s^2 and g_s , respectively, are only partially known by now (see [15–17] for the details of the provided NLL contributions and [42] for a recent summary).

In the present paper, we calculate $\mathcal{O}(\alpha_s)$ corrections arising from the self-interference contribution of the electromagnetic dipole operator \mathcal{O}_7 to the double differential decay width $d\Gamma/(ds_1 ds_2)$ for $\bar{B} \rightarrow X_s\gamma\gamma$, where the kinematical variables s_1 and s_2 are defined as $s_i = (p_b - q_i)^2/m_b^2$ with

p_b, q_1, q_2 being the four-momenta of the b -quark and two photons. At this order in α_s , this involves contributions with three (virtual) and four particles (bremsstrahlung) in the final state. The key difference to our study in Ref. [16] is that we keep the *full* dependence on strange-quark mass in our results.

Kinematically, the (s_1, s_2) -region accessible to the three body decay $b \rightarrow s\gamma\gamma$ is given by (see [43]) by²

$$\begin{aligned} s_1 > x_4, \quad s_2 > x_4, \quad 1 - s_1 - s_2 + x_4 > 0; \\ s_1 s_2 > x_4, \end{aligned} \quad (3)$$

where $x_4 = m_s^2/m_b^2$. In the rest frame of the decaying b -quark, one has a simple relation between s_i variables and final state photon energies E_i : $s_i = 1 - 2E_i/m_b$. At this stage, we need to impose some kinematical cuts. First, in order for observing two hard photons, the s_i variables should be smaller than one. Also, detection of two distinct photons requires kinematically that their invariant mass is different from zero. It is possible to satisfy all these requirements using a single physical cutoff parameter c ($c > x_4$), by demanding³

$$1 - s_1 - s_2 > c; \quad (s_1 - c)(s_2 - c) > c. \quad (4)$$

Note that the region defined in Eq. (4) is a subregion of the one specified in Eq. (3).

With these cuts at hand, soft photon related singularities are absent, whereas there exist kinematical configurations where one of the photons can become collinear to the s -quark. Working with a finite strange quark mass our final NLL result involves single logarithms of the form $\log(m_s/m_b)$, whose origin is entirely related to collinear photon emissions from s -quark and *not* to gluons. The reason for this is that QCD-wise, our observable (the double or triple differential decay width) is fully inclusive and therefore nonsingular. As a result, all soft and/or collinear gluon related singularities cancel out in our final result after adding the corresponding virtual and bremsstrahlung corrections, as a consequence of the Kinoshita-Lee-Nauenberg (KLN) theorem. However, QED-wise our observable is not fully inclusive, because we want to observe exactly two photons in the final state; therefore $\log(m_s/m_b)$ terms remain.

We note that m_s , which is initially introduced as an infrared/collinear regulator, is eventually interpreted to be

²The phase-space region corresponding to real gluon radiation $b \rightarrow sg\gamma\gamma$ is wider than this. Nevertheless we consider the bremsstrahlung process only in the restricted region, which is also accessible to the three body decay $b \rightarrow s\gamma\gamma$.

³In terms of the four particle final state, the invariant mass squared $s = (q_1 + q_2)^2/m_b^2$ of the two photons can be written as $s = 1 - s_1 - s_2 + s_3$, where s_3 is the normalized hadronic mass squared. Then, choosing $1 - s_1 - s_2 > c$, still prevents the photons from flying parallel to each other.

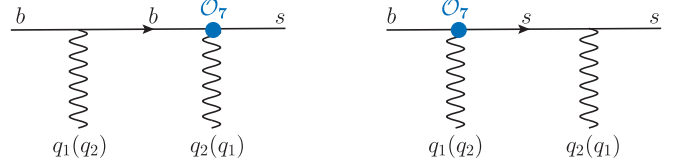


FIG. 1. Tree-level amplitudes representing the $(\mathcal{O}_7, \mathcal{O}_7)$ contribution to $b \rightarrow s\gamma\gamma$. The symmetric diagrams are understood to be obtained from those shown by interchanging q_1 with q_2 as indicated in brackets.

a mass of constituent type varying between 400–600 MeV in the final numerics. We believe that this range covers the nonperturbative uncertainties due to the hadronic substructure of photons. This approach has also been adopted previously, e.g. by Kaminski *et al.* in [44] and Asatrian *et al.* in [16,17,45]. The experience gained in these references shows that the constituent mass approach gives results which are similar to those when using fragmentation functions [45]. Therefore, we believe that this method is sufficient to obtain an estimate of the calculated contribution. While the fragmentation approach seems better from the theoretical point of view, it is not clear that it leads to better final results in practice, because the fragmentation functions (for $s \rightarrow \gamma$ or $g \rightarrow \gamma$) suffer from experimental uncertainties, as pointed out in [45]. An alternative could be to look at the version with “isolated photons” a la Frixione [46] which corresponds, however, to a slightly different observable. Such an approach is beyond the scope of the present paper and is left for future studies.

III. IMPROVED LEADING ORDER RESULTS

In this section we give the double differential decay width $d\Gamma/(ds_1 ds_2)$ at lowest order in QCD, keeping the full dependence on the strange quark mass. We define the dimensionless variables s_1 and s_2 as

$$s_1 = \frac{(p_b - q_1)^2}{m_b^2}; \quad s_2 = \frac{(p_b - q_2)^2}{m_b^2}. \quad (5)$$

At lowest order the double differential decay width $d\Gamma_{77}^{(0,d)}/(ds_1 ds_2)$ is based on the diagrams shown in Fig. 1. Since the lowest order decay width will also be needed for the UV-renormalization of the virtual corrections, we present the leading-order result in $d = 4 - 2\epsilon$ dimensions, keeping terms up to ϵ^1 order in the expansion. Using $x_4 = m_s^2/m_b^2$, we obtain

$$\frac{d\Gamma_{77}^{(0,d)}}{ds_1 ds_2} = \frac{\alpha^2 m_b^3 |C_{7,\text{eff}}(\mu)|^2 G_F^2 |V_{tb} V_{ts}^*|^2 Q_d^2}{1024\pi^5} \left(\frac{\mu}{m_b}\right)^{4\epsilon} \tilde{r}, \quad (6)$$

with

$$\tilde{r} = \frac{[\bar{m}_b^2(\mu)\tilde{r}_a + \sqrt{x_4}\bar{m}_s(\mu)\bar{m}_b(\mu)\tilde{r}_b + \bar{m}_s^2(\mu)\tilde{r}_c + \epsilon m_b^2(\tilde{r}_1 + \tilde{r}_2 + \tilde{r}_3)](1 - s_1 - s_2 + x_4)}{(1 - s_1)^2(s_1 - x_4)^2(1 - s_2)^2(s_2 - x_4)^2}. \quad (7)$$

Note that the terms proportional to ϵ in Eq. (7) will only be involved in the renormalization procedure of the virtual corrections, leading there to terms of order α_s . As in such terms the running masses $\bar{m}_b(\mu)$ and $\bar{m}_s(\mu)$ can be identified with the pole masses m_b and m_s , we immediately performed this identification in the corresponding terms of Eq. (7).

The individual \tilde{r}_i quantities read

$$\begin{aligned} \tilde{r}_a &= 8(s_1^2s_2 + s_1^4s_2 + s_1s_2^2 - 12s_1^2s_2^2 + 14s_1^3s_2^2 - 7s_1^4s_2^2 + 14s_1^2s_2^3 - 24s_1^3s_2^3 + 12s_1^4s_2^3 + s_1s_2^4 - 7s_1^2s_2^4 + 12s_1^3s_2^4 \\ &\quad - 6s_1^4s_2^4 - 3s_1^2x_4 + 2s_1^3x_4 - s_1^4x_4 - 2s_1s_2x_4 + 23s_1^2s_2x_4 - 38s_1^3s_2x_4 + 13s_1^4s_2x_4 - 3s_2^2x_4 + 23s_1s_2^2x_4 \\ &\quad - 50s_1^2s_2^2x_4 + 68s_1^3s_2^2x_4 - 24s_1^4s_2^2x_4 + 2s_2^3x_4 - 38s_1s_2^3x_4 + 68s_1^2s_2^3x_4 - 52s_1^3s_2^3x_4 + 12s_1^4s_2^3x_4 - s_2^4x_4 \\ &\quad + 13s_1s_2^4x_4 - 24s_1^2s_2^4x_4 + 12s_1^3s_2^4x_4 + 5s_1x_4^2 - 7s_1^2x_4^2 + 16s_1^3x_4^2 - 6s_1^4x_4^2 + 5s_2x_4^2 - 56s_1s_2x_4^2 + 82s_1^2s_2x_4^2 \\ &\quad - 48s_1^3s_2x_4^2 + 13s_1^4s_2x_4^2 - 7s_2^2x_4^2 + 82s_1s_2^2x_4^2 - 152s_1^2s_2^2x_4^2 + 68s_1^3s_2^2x_4^2 - 7s_1^4s_2^2x_4^2 + 16s_2^3x_4^2 - 48s_1s_2^3x_4^2 \\ &\quad + 68s_1^2s_2^3x_4^2 - 24s_1^3s_2^3x_4^2 - 6s_2^4x_4^2 + 13s_1s_2^4x_4^2 - 7s_1^2s_2^4x_4^2 - 4x_4^3 + 19s_1x_4^3 - 42s_1^2x_4^3 + 16s_1^3x_4^3 - s_1^4x_4^3 + 19s_2x_4^3 \\ &\quad - 48s_1s_2x_4^3 + 82s_1^2s_2x_4^3 - 38s_1^3s_2x_4^3 + s_1^4s_2x_4^3 - 42s_2^2x_4^3 + 82s_1s_2^2x_4^3 - 50s_1^2s_2^2x_4^3 + 14s_1^3s_2^2x_4^3 + 16s_2^3x_4^3 \\ &\quad - 38s_1s_2^3x_4^3 + 14s_1^2s_2^3x_4^3 - s_2^4x_4^3 + s_1s_2^4x_4^3 - 6x_4^4 + 19s_1x_4^4 - 7s_1^2x_4^4 + 2s_1^3x_4^4 + 19s_2x_4^4 - 56s_1s_2x_4^4 + 23s_1^2s_2x_4^4 \\ &\quad - 7s_2^2x_4^4 + 23s_1s_2^2x_4^4 - 12s_1^2s_2^2x_4^4 + 2s_2^3x_4^4 - 4x_4^5 + 5s_1x_4^5 - 3s_1^2x_4^5 + 5s_2x_4^5 - 2s_1s_2x_4^5 + s_1^2s_2x_4^5 - 3s_2^2x_4^5 + s_1s_2^2x_4^5), \\ \tilde{r}_b &= -32(1 - s_1)(1 - s_2)(s_1 - x_4)(s_2 - x_4)(s_1s_2 - x_4)(1 + x_4 - s_1 - s_2), \\ \tilde{r}_c &= \tilde{r}_a, \end{aligned} \quad (8)$$

$$\begin{aligned} \tilde{r}_1 &= -16s_1^2x_4^6 - 16s_2^2x_4^6 - 16s_1x_4^6 + 48s_1s_2x_4^6 - 16s_2x_4^6 + 16x_4^6 + 16s_1s_2^3x_4^5 + 144s_1^2x_4^5 - 16s_1^2s_2^2x_4^5 - 112s_1s_2^2x_4^5 \\ &\quad + 144s_2^2x_4^5 - 208s_1x_4^5 + 16s_1^3s_2x_4^5 - 112s_1^2s_2x_4^5 + 224s_1s_2x_4^5 - 208s_2x_4^5 + 112x_4^5 - 144s_1^3x_4^4 - 32s_1^2s_2^3x_4^4 + 128s_1s_2^3x_4^4 \\ &\quad - 144s_2^3x_4^4 + 448s_1^2x_4^4 - 32s_1^3s_2^2x_4^4 + 576s_1^2s_2^2x_4^4 - 928s_1s_2^2x_4^4 + 448s_2^2x_4^4 - 448s_1x_4^4 + 128s_1^3s_2x_4^4 - 928s_1^2s_2x_4^4 \\ &\quad + 1264s_1s_2x_4^4 - 448s_2x_4^4 + 112x_4^4 + 64s_1^4x_4^3 + 16s_1^2s_2^4x_4^3 - 80s_1s_2^4x_4^3 + 64s_2^4x_4^3 - 352s_1^3x_4^3 + 48s_1^3s_2^3x_4^3 - 544s_1^2s_2^3x_4^3 \\ &\quad + 880s_1s_2^3x_4^3 - 352s_2^3x_4^3 + 448s_1^2x_4^3 + 16s_1^4s_2^2x_4^3 - 544s_1^3s_2^2x_4^3 + 1744s_1^2s_2^2x_4^3 - 1760s_1s_2^2x_4^3 + 448s_2^2x_4^3 - 208s_1x_4^3 \\ &\quad - 80s_1^4s_2x_4^3 + 880s_1^3s_2x_4^3 - 1760s_1^2s_2x_4^3 + 1264s_1s_2x_4^3 - 208s_2x_4^3 + 16x_4^3 + 64s_1^4x_4^2 - 16s_1^3s_2^4x_4^2 + 176s_1^2s_2^4x_4^2 \\ &\quad - 224s_1s_2^4x_4^2 + 64s_2^4x_4^2 - 144s_1^3x_4^2 - 16s_1^4s_2^2x_4^2 + 464s_1^3s_2^2x_4^2 - 1152s_1^2s_2^2x_4^2 + 880s_1s_2^2x_4^2 - 144s_2^2x_4^2 + 144s_1^2x_4^2 \\ &\quad + 176s_1^4s_2^2x_4^2 - 1152s_1^3s_2^2x_4^2 + 1744s_1^2s_2^2x_4^2 - 928s_1s_2^2x_4^2 + 144s_2^2x_4^2 - 16s_1x_4^2 - 224s_1^4s_2x_4^2 + 880s_1^3s_2x_4^2 - 928s_1^2s_2x_4^2 \\ &\quad + 224s_1s_2x_4^2 - 16s_2x_4^2 - 96s_1^3s_2^4x_4 + 176s_1^2s_2^4x_4 - 80s_1s_2^4x_4 - 96s_1^4s_2^3x_4 + 464s_1^3s_2^3x_4 - 544s_1^2s_2^3x_4 + 128s_1s_2^3x_4 \\ &\quad - 16s_2^3x_4 + 176s_1^4s_2^2x_4 - 544s_1^3s_2^2x_4 + 576s_1^2s_2^2x_4 - 112s_1s_2^2x_4 - 16s_2^2x_4 - 80s_1^4s_2x_4 + 128s_1^3s_2x_4 - 112s_1^2s_2x_4 \\ &\quad + 48s_1s_2x_4 - 16s_1^3s_2^4 + 16s_1^2s_2^4 - 16s_1^4s_2^3 + 48s_1^3s_2^3 - 32s_1^2s_2^3 + 16s_1s_2^3 + 16s_1^4s_2^2 - 32s_1^3s_2^2 - 16s_1^2s_2^2 + 16s_1^3s_2, \\ \tilde{r}_2 &= -\tilde{r}_0 \log(s_1s_2 - x_4), \\ \tilde{r}_3 &= -\tilde{r}_0 \log(1 - s_1 - s_2 + x_4), \tilde{r}_0 = \tilde{r}_a + x_4(\tilde{r}_b + \tilde{r}_c). \end{aligned}$$

The leading-order spectrum in $d = 4$ dimensions is simply understood to be obtained from Eq. (6) and Eq. (7) by setting ϵ to zero. In the limit $m_s \rightarrow 0$, Eq. (6) correctly reproduces the tree-level result given in Eq. (2.3) of Ref. [16], which was derived in this limit.

For completeness, we have also improved the lowest order results for the double differential decay width based on the remaining operators \mathcal{O}_1 and \mathcal{O}_2 by working out the full m_s dependence. For this piece we obtain⁴

⁴Note that in Eq. (2.10) of Ref. [16] there was a sign mistake which is corrected in Eq. (9) of the present work.

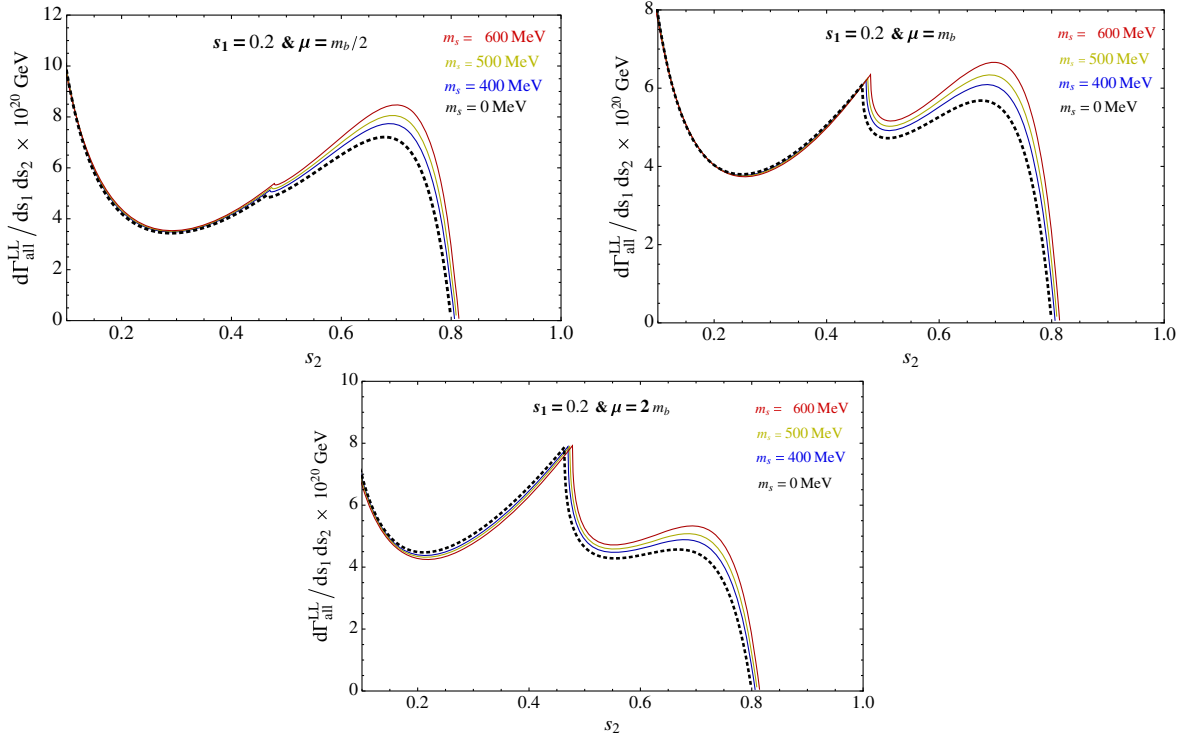


FIG. 2. Leading-order spectrum based on all operator contributions as given in Eq. (6) and Eq. (9), as a function of s_2 for s_1 fixed at 0.2 and $\mu \in [m_b/2, 2m_b]$. The dotted (lowermost), blue, yellow and red (uppermost) lines in these frames describe the results when putting $m_s = 0$, $m_s = 400$ MeV, $m_s = 500$ MeV and $m_s = 600$ MeV, respectively.

$$\frac{d\Gamma_{\text{Remaining}}^{(0)}}{ds_1 ds_2} = \frac{\alpha^2 m_b^5 G_F^2 |V_{tb} V_{ts}^*|^2}{1024\pi^5} \times \left\{ 4Q_u^4 \left(C_2(\mu) + \frac{4}{3} C_1(\mu) \right)^2 \frac{(s_1 + s_2 - (4 - s_1 - s_2)x_4)}{(1 - s_1 - s_2 + x_4)^2} \tilde{h}_{(2,1)} \right. \\ \left. - 16Q_u^2 Q_d \left(C_2(\mu) + \frac{4}{3} C_1(\mu) \right) C_{7,\text{eff}}(\mu) \frac{1}{(1 - s_1)(1 - s_2)(s_1 - x_4)(s_2 - x_4)} \tilde{h}_{(2,1,7)} \right\}. \quad (9)$$

The \tilde{h} functions appearing in Eq. (9) read

$$\tilde{h}_{(2,1)} = |1 - s_1 - s_2 + x_4 - 4\hat{m}_c^2 \arcsin^2(\tilde{z})|^2, \quad (10)$$

$$\tilde{h}_{(2,1,7)} = (s_1 s_2 x_4^3 - 2s_1 x_4^3 - 2s_2 x_4^3 + 2s_1^2 x_4^2 - s_1 s_2^2 x_4^2 + 2s_2^2 x_4^2 - 6s_1 x_4^2 - s_1^2 s_2 x_4^2 + 7s_1 s_2 x_4^2 - 6s_2 x_4^2 + 2s_1^2 x_4 \\ + s_1^2 s_2^2 x_4 - 4s_1 s_2^2 x_4 + 2s_2^2 x_4 - 2s_1 x_4 - 4s_1^2 s_2 x_4 + 7s_1 s_2 x_4 - 2s_2 x_4 + s_1^2 s_2^2 - s_1 s_2^2 - s_1^2 s_2 + s_1 s_2 \\ + 3x_4^3 + 3x_4^2)(1 - s_1 - s_2 + x_4 - 4\hat{m}_c^2 \text{Re}[\arcsin^2(\tilde{z})]), \quad (11)$$

where $\hat{m}_c = m_c/m_b$. The argument of the arcsin function reads $\tilde{z} = \sqrt{(1 - s_1 - s_2 + x_4)/(4\hat{m}_c^2)}$, where \hat{m}_c^2 is tacitly understood to have a small negative imaginary part. In Fig. 2 we present the leading-order spectrum based on all operators [see Eq. (6) and Eq. (9)] as a function of s_2 for s_1 fixed at 0.2 and $\mu \in [m_b/2, 2m_b]$. The dotted (lowermost), blue, yellow and red (uppermost) lines in these frames describe the results when putting $m_s = 0$, $m_s = 400$ MeV,

$m_s = 500$ MeV and $m_s = 600$ MeV, respectively. The numerical values of the input parameters and of the Wilson coefficients are listed in Table I. We see that for $\mu = m_b/2$ the $(\mathcal{O}_7, \mathcal{O}_7)$ contribution is by far the dominant one. This can be easily understood from Eq. (9). For the renormalization scale $\mu = m_b/2$ the combination $(C_2(\mu) + \frac{4}{3}C_1(\mu))$ tends to zero since $C_2(m_b/2) \approx -\frac{4}{3}C_1(m_b/2)$ and thus the $(\mathcal{O}_7, \mathcal{O}_7)$ contribution dominates at this scale.

TABLE I. Top: Input parameters used in this paper. Bottom: Relevant Wilson coefficients and $\alpha_s(\mu)$ at different values of the renormalization scale μ .

Parameter	Value
$\text{BR}_{sl}^{\text{exp}}$	0.1049
m_c/m_b	0.29
m_b	4.8 GeV
m_t	175 GeV
m_W	80.4 GeV
m_Z	91.19 GeV
G_F	$1.16637 \times 10^{-5} \text{ GeV}^{-2}$
V_{cb}	0.04
$V_{tb}V_{ts}^*$	0.04
$\alpha_{\text{(em)}}^{-1}$	137
$\alpha_s(m_Z)$	0.119

	$C_1^0(\mu)$	$C_2^0(\mu)$	$C_{7,\text{eff}}^0(\mu)$	$C_{7,\text{eff}}^1(\mu)$	$\alpha_s(\mu)$
$\mu = m_W$	0	1	-0.1957	-2.3835	0.1213
$\mu = 2m_b$	-0.3352	1.0116	-0.2796	-0.1788	0.1818
$\mu = m_b$	-0.4976	1.0245	-0.3142	0.4728	0.2175
$\mu = m_b/2$	-0.7117	1.0478	-0.3556	1.0794	0.2714

IV. IMPROVED $\mathcal{O}(\alpha_s)$ RESULTS FOR THE DOUBLE DIFFERENTIAL SPECTRUM $d\Gamma/(ds_1 ds_2)$

A. Virtual corrections

We now turn to the calculation of the virtual QCD corrections, i.e., to the contributions of order α_s with three particles in the final state. The diagrams defining the

(unrenormalized) virtual corrections at the amplitude level are shown in the first two lines of Fig. 3. As the diagrams with a self-energy insertion on the external b - and s -quark legs are taken into account in the renormalization process, these diagrams are not shown in Fig. 3. In order to get the (unrenormalized) virtual corrections $d\Gamma_{77}^{\text{bare}}/(ds_1 ds_2)$ of order α_s , we have to work out the interference of the diagrams in Fig. 3 with the leading order diagrams in Fig. 1.

From the technical point of view we use two different methods to perform the calculations. In the first method we use the Laporta Algorithm [47] (see also [48,49]) to identify the needed master integrals, followed by applying the differential equation method to solve them. As we used these techniques also in [15], we refer to Sec. 7 of that paper which contains the technical details and the corresponding references. In the second method, the one-loop amplitudes are reduced to tensor integrals and subsequently decomposed into their Lorentz-covariant structure by means of the *Mathematica* package FEYNALCALC [50,51]. For the numerical evaluation of the tensor-coefficient functions we employed the LOOPTOOLS library [52,53]. For some checks, we also used the SecDec-3.0 package [54]. We note that the two methods give the same result, providing us with firm check of our results.

In order to renormalize the calculated bare $\mathcal{O}(\alpha_s)$ virtual corrections, one needs to add counterterm contributions which, in our case, can be divided into two parts as

$$\frac{d\Gamma_{77}^{\text{ct}}}{ds_1 ds_2} = \frac{d\Gamma_{77}^{\text{ct,(A)}}}{ds_1 ds_2} + \frac{d\Gamma_{77}^{\text{ct,(B)}}}{ds_1 ds_2}. \quad (12)$$

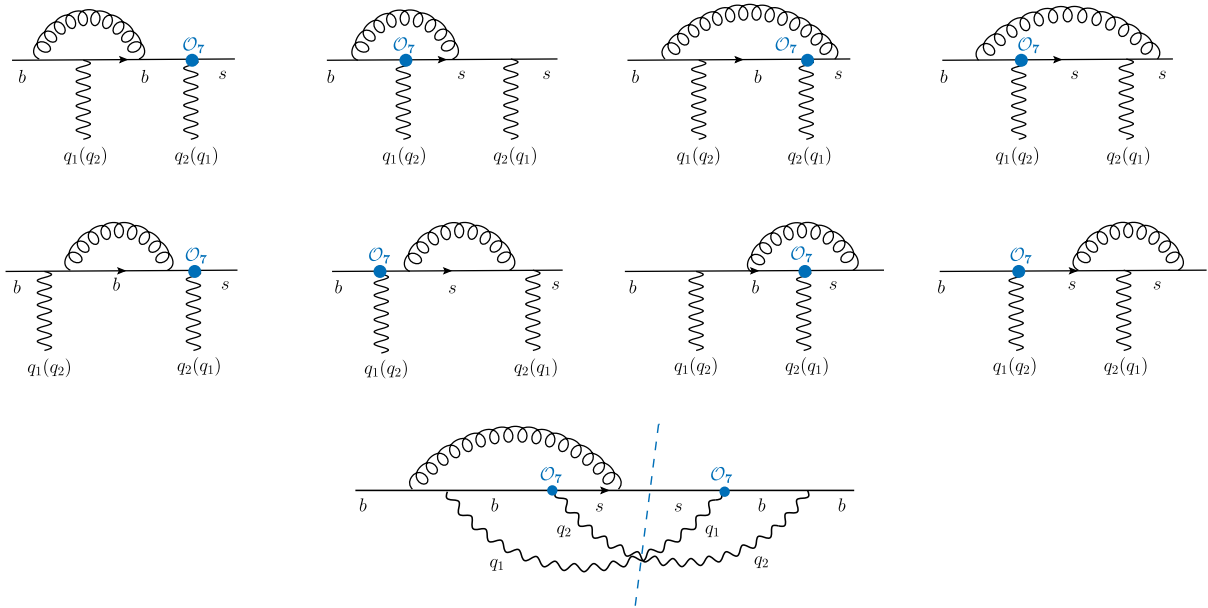


FIG. 3. On the first two lines the one-loop Feynman diagrams for $b \rightarrow s\gamma\gamma$ associated with \mathcal{O}_7 are shown at the amplitude level. Diagrams with self-energy insertions on the external quark-legs are not shown. On the last line the contribution to the decay width corresponding to the interference of the third diagram on the first line with the first (tree-level) diagram in Fig. 1 with $q_1 \leftrightarrow q_2$ is shown.

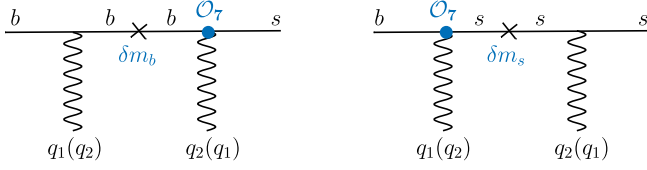


FIG. 4. Counterterm amplitudes involving $\delta m_{s,b}$ insertions in the internal quark lines.

Part (A) involves the Lehmann, Symanzik, Zimmermann (LSZ) factors $\sqrt{Z_{2b}^{\text{OS}}}$ and $\sqrt{Z_{2s}^{\text{OS}}}$ for the b - and s -quark fields, as well as the self-renormalization constant $Z_{77}^{\overline{\text{MS}}}$ of the operator \mathcal{O}_7 , as well as $Z_{m_b}^{\overline{\text{MS}}}$ and $Z_{m_s}^{\overline{\text{MS}}}$ renormalizing the factors $\bar{m}_b(\mu)$ and $\bar{m}_s(\mu)$ present in the operator \mathcal{O}_7 . Defining $\delta Z_i = Z_i - 1$, we get for part (A)

$$\frac{d\Gamma_{77}^{\text{ct,(A)}}}{ds_1 ds_2} = [\delta Z_{2b}^{\text{OS}} + \delta Z_{2s}^{\text{OS}} + 2\delta Z_m^{\overline{\text{MS}}} + 2\delta Z_{77}^{\overline{\text{MS}}}] \frac{d\Gamma_{77}^{(0,d)}}{ds_1 ds_2}. \quad (13)$$

The simple structure of this result is related to the fact that the $\overline{\text{MS}}$ renormalization constants of the bottom and the strange quark mass are identical, i.e., $Z_{m_b}^{\overline{\text{MS}}} = Z_{m_s}^{\overline{\text{MS}}} \equiv Z_m^{\overline{\text{MS}}}$.

The counterterms defining part (B) are due to the insertion of $-i\delta m_b \bar{b}b$ and $-i\delta m_s \bar{s}s$ in the internal b and s -quark lines in the leading order diagrams as indicated in Fig. 4, where

$$\delta m_b = (Z_{m_b}^{\text{OS}} - 1)m_b, \quad \delta m_s = (Z_{m_s}^{\text{OS}} - 1)m_s.$$

More precisely, part (B) consists of the interference of the diagrams in Fig. 4 with the leading order diagrams in Fig. 1. The various Z -factors are listed for completeness in Appendix B.

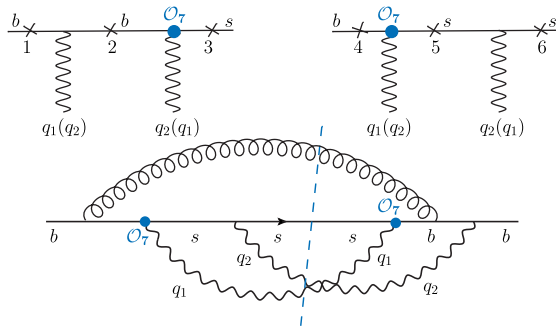


FIG. 5. On the first line the diagrams defining the \mathcal{O}_7 contribution to $b \rightarrow s\gamma\gamma$ are shown at the amplitude level. The crosses in the graphs stand for the possible emission places of the gluon. On the second line the contribution to the decay width corresponding to the interference of diagram 4 with diagram 2 ($q_1 \leftrightarrow q_2$) is illustrated. This sample interference diagram gives rise to $\log(m_s/m_b)$ terms due to collinear configurations of one of the photons with the s -quark.

By adding $d\Gamma_{77}^{\text{bare}}/(ds_1 ds_2)$ and $d\Gamma_{77}^{\text{ct}}/(ds_1 ds_2)$, we get the result for the renormalized virtual corrections to the spectrum, $d\Gamma_{77}^{(1),\text{virt}}/(ds_1 ds_2)$.

$$\frac{d\Gamma_{77}^{(1),\text{virt}}}{ds_1 ds_2} = \frac{d\Gamma_{77}^{\text{bare}}}{ds_1 ds_2} + \frac{d\Gamma_{77}^{\text{ct}}}{ds_1 ds_2}. \quad (14)$$

B. Bremsstrahlung corrections

We now turn to the calculation of the bremsstrahlung QCD corrections, i.e., to the contributions of order α_s with four particles in the final state. The corresponding diagrams at the amplitude level are shown on the first line in Fig. 5. We use again two methods to calculate the bremsstrahlung corrections. In the first one, we use the Laporta Algorithm [47] to identify the master integrals, which are then solved by applying the differential equation method. As in [45] we worked out in a first step the triple differential spectrum $d\Gamma_{77}^{(1),\text{brems}}/(ds_1 ds_2 ds_3)$, $s_3 = (p_s + p_g)^2/m_b^2$, obtaining a fully analytic result which however is very lengthy. To get the double differential spectrum $d\Gamma_{77}^{(1),\text{brems}}/ds_1 ds_2$, we integrated over s_3 , which runs in the interval $[m_s^2/m_b^2, s_1 s_2]$. In some terms this integration was done numerically. In the second method we perform a slicing of the phase-space: We introduce a small gluon energy cutoff ω_0 and divide the real emission contribution into a *soft* and a *hard* part. The soft part, which contains the infrared (IR) singularity, comes from the phase space region where the gluon energy is below ω_0 . As in the case of the virtual diagrams, the IR singularities are regularized dimensionally. By taking advantage of the soft gluon approximation for the amplitude of the bremsstrahlung process, it is possible to perform the integral with respect to the gluon momentum analytically; the process-independent result, which was derived in [55] (see also [56]), depends only on the momenta of the external particles in the corresponding Born process. We explicitly checked that the IR divergencies cancel out once the soft part is combined with the virtual corrections. In order to obtain the hard part contribution to the double differential decay width, a three-dimensional (finite) integral is involved; we performed this integration numerically, by making use of the CUBA-library [57]. Again, the two methods lead to the same result.

C. Improved final result for the decay width at $\mathcal{O}(\alpha_s)$

The complete order α_s correction to the double differential decay width $d\Gamma_{77}/(ds_1 ds_2)$ is obtained by adding the renormalized virtual corrections from Sec. IV A and the bremsstrahlung corrections discussed in Sec. IV B:

$$\frac{d\Gamma_{77}^1}{ds_1 ds_2} = \frac{d\Gamma_{77}^{(1),\text{virt}}}{ds_1 ds_2} + \frac{d\Gamma_{77}^{(1),\text{brems}}}{ds_1 ds_2}. \quad (15)$$

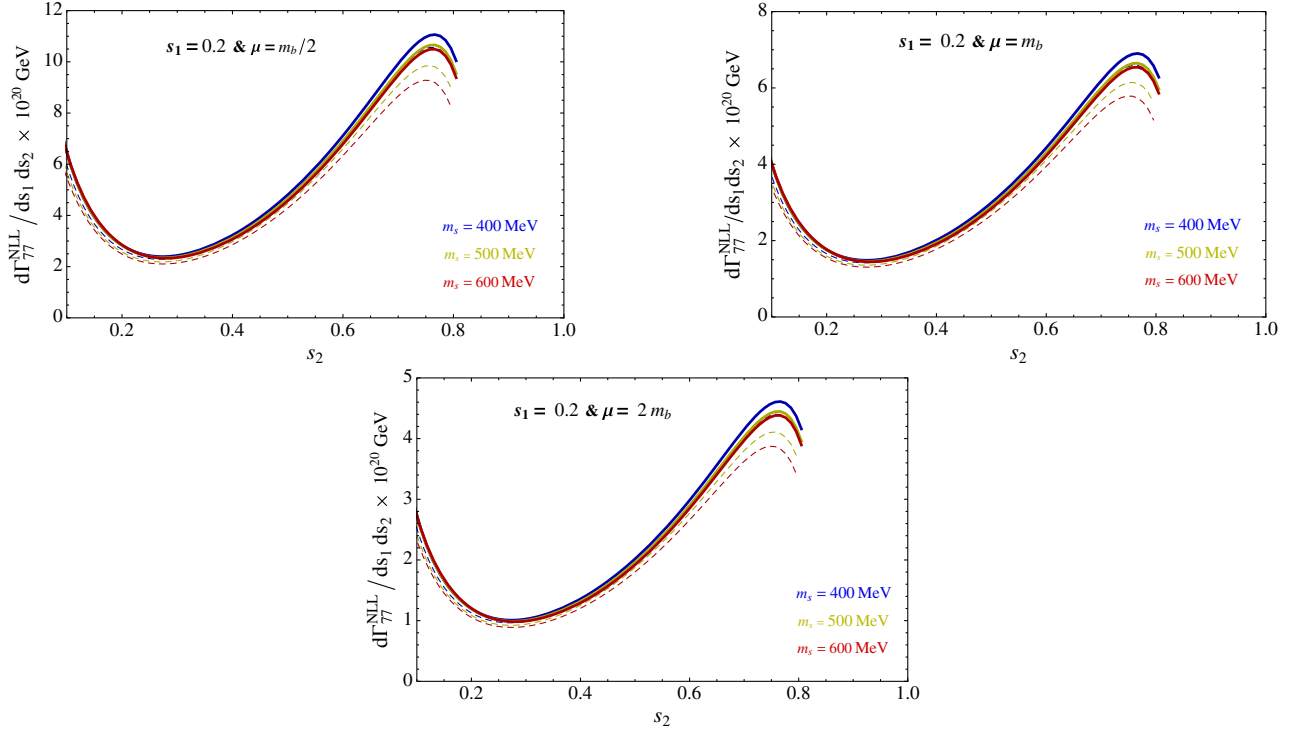


FIG. 6. NLL double differential spectrum based on $(\mathcal{O}_7, \mathcal{O}_7)$ contribution only, as a function of s_2 for s_1 fixed at 0.2. In each of these plots, the solid curves show the results based on the new calculation with exact m_s , while the dashed curves are based on previous results, i.e., in the limit $m_s \rightarrow 0$. See the text for details.

V. NUMERICAL ILLUSTRATIONS

The NLL prediction for the double differential decay width reads

$$\frac{d\Gamma_{77}}{ds_1 ds_2} = \frac{d\Gamma_{77}^{(0,4)}}{ds_1 ds_2} + \frac{d\Gamma_{77}^{(1)}}{ds_1 ds_2}. \quad (16)$$

To illustrate our results, we first rewrite the $\overline{\text{MS}}$ masses $\bar{m}_b(\mu)$, $\bar{m}_s(\mu)$ in Eq. (16) in terms of the pole masses m_b , m_s , using the one-loop relations

$$\bar{m}_b(\mu) = m_b \left[1 - \frac{\alpha_s(\mu)}{4\pi} \left(8 \log \frac{\mu}{m_b} + \frac{16}{3} \right) \right], \quad (17)$$

$$\bar{m}_s(\mu) = m_s \left[1 - \frac{\alpha_s(\mu)}{4\pi} \left(8 \log \frac{\mu}{m_s} + \frac{16}{3} \right) \right]. \quad (18)$$

We then insert $C_{7,\text{eff}}(\mu)$ in the form

$$C_{7,\text{eff}}(\mu) = C_{7,\text{eff}}^0(\mu) + \frac{\alpha_s(\mu)}{4\pi} C_{7,\text{eff}}^1(\mu) \quad (19)$$

and expand the resulting expression for $d\Gamma_{77}/(ds_1 ds_2)$ with respect to α_s , discarding terms of order α_s^2 . This procedure defines the NLL result. The corresponding LL result is obtained by discarding the order α_s^1 terms. The numerical values for the input parameters and for the Wilson coefficient $C_{7,\text{eff}}(\mu)$ at various values for the scale

μ , together with the numerical values of $\alpha_s(\mu)$, are given in Table I.

In Fig. 6 we give the NLL double differential spectrum based on the $(\mathcal{O}_7, \mathcal{O}_7)$ contribution only, as a function of s_2 for s_1 fixed at 0.2. In each of these plots, the solid curves show the results based on the present calculation with exact m_s dependence, while the dashed curves are based on the previous approximated result of Ref. [16], where only logarithmic and constant terms in m_s were kept (which we denote as “ $m_s \rightarrow 0$ results”). The renormalization scale μ and m_s are varied as explicitly displayed. A straightforward comparison between the solid (m_s exact results) and the dashed curves ($m_s \rightarrow 0$ results) shows that finite m_s effects are only sizable near the kinematical endpoints of the spectrum. One also can see that the exact m_s results only develop a sizable m_s dependence near the kinematical endpoints of the spectrum.

In Fig. 7 we give the NLL double differential spectrum based on all available operator contributions to date as a function of s_2 (for s_1 fixed at 0.2) taking $\mu \in \{m_b/2, m_b, 2m_b\}$ and putting $m_s = 400$ MeV, $m_s = 500$ MeV, and $m_s = 600$ MeV.

We stress that the numerically important QCD corrections to the matrix element for $\bar{B} \rightarrow X_s \gamma \gamma$ involving the operators \mathcal{O}_1 and \mathcal{O}_2 are unknown so far. Our calculation based on the operator \mathcal{O}_7 therefore only represents a partial next-to-leading logarithmic (NLL) result. In general, a reduction of the scale dependence is not expected at this

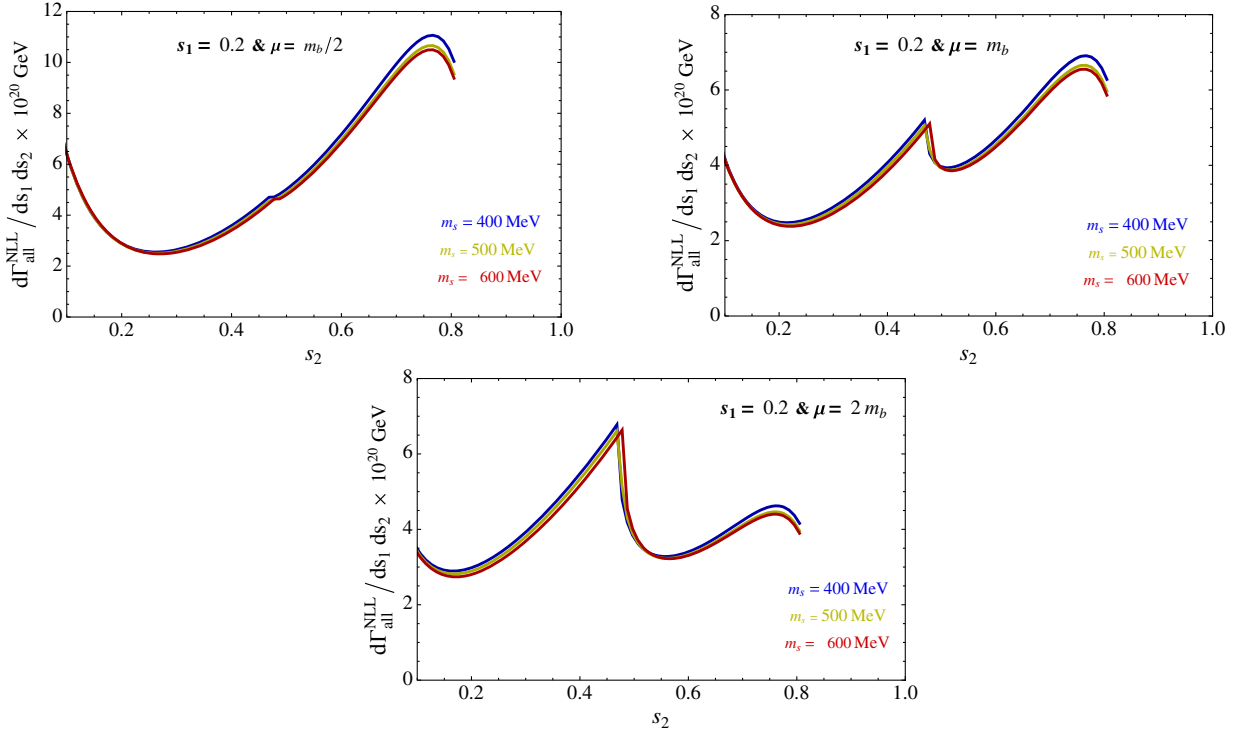


FIG. 7. NLL spectrum (with exact treatment of m_s) based on all available operator contributions to date, as a function of s_2 for s_1 fixed at 0.2. The blue (uppermost), yellow, and red (lowermost) curves in these frames describe the results when putting $m_s = 400$ MeV, $m_s = 500$ MeV, and $m_s = 600$ MeV, respectively.

level. Indeed, we find that our partial NLL result shows a similar scale dependence as leading logarithmic (LL) result. Historically, a similar feature was observed in the process $B \rightarrow X_s \gamma$. Partial NLL results for the branching ratio showed a scale dependence similar to the one at LL. Only after taking into account all NLL contributions, the scale dependence got drastically reduced.

As the analytic expressions for the double differential decay width $d\Gamma(B \rightarrow X_s \gamma\gamma)/(ds_1 ds_2)$ are very lengthy, they cannot be given in this paper. In order to provide nevertheless the complete information, we decided to give it in form of a Fortran program, called “doublediff.F”, which can be obtained from the authors. The input/output information is described in a few comment lines at the beginning of the very short main program. The program uses the LOOPTOOLS-library [52,53] and the CUBA-library [57]. The code has been tested when using the versions LoopTools-2-13 and Cuba-3.2, respectively.

We already mentioned that one gets a sizable m_s dependence only near the kinematical endpoints of the spectrum. This means that if one is sufficiently away from these endpoints, one gets more reliable predictions. From Eq. (4) one can see that this situation can be achieved when choosing a value for c which is not too small. On the other hand, the decay width for $\bar{B} \rightarrow X_s \gamma\gamma$ will decrease for increasing values of c . It is therefore necessary to take compromising values for c . Explicit calculations show that for $c = 1/50$ the decay width does not develop a sizable m_s

dependence: When varying m_s between 400 and 600 MeV, the impact on the decay width is less than 5%. For larger choices of c , the m_s sensitivity is even much smaller. To illustrate the c -dependence of the decay width, we use the values $c = 1/50$, $c = 1/25$ and $c = 1/15$ in the following.

In the decay $B \rightarrow X_s \gamma\gamma$ two photons are emitted, characterized by the kinematical variables s_1 and s_2 . We now define the one-dimensional physical spectrum

$$\frac{d\Gamma_{77}}{ds} \quad \text{where } s = \min\{s_1, s_2\}. \quad (20)$$

This observable can be constructed from the double differential spectrum $d\Gamma_{77}/(ds_1 ds_2)$ in the following way:

$$\frac{d\Gamma_{77}}{ds} = 2 \left[\int_G ds_2 d\Gamma_{77}/(ds_1 ds_2) \right]_{s_1 \rightarrow s}. \quad (21)$$

The integration interval G can be specified as follows: For a given value of s_1 the variable s_2 runs over all values in the cut phase space [characterized by Eq. (4)] which satisfy the additional condition $s_2 > s_1$. More explicitly, this can be summarized as

$$\frac{1}{2}(1 - c - \sqrt{1 - 10c + 9c^2}) < s_1 < \frac{1}{2}(1 - c);$$

$$\max \left\{ s_1, c + \frac{c}{s_1 - c} \right\} < s_2 < 1 - c - s_1. \quad (22)$$

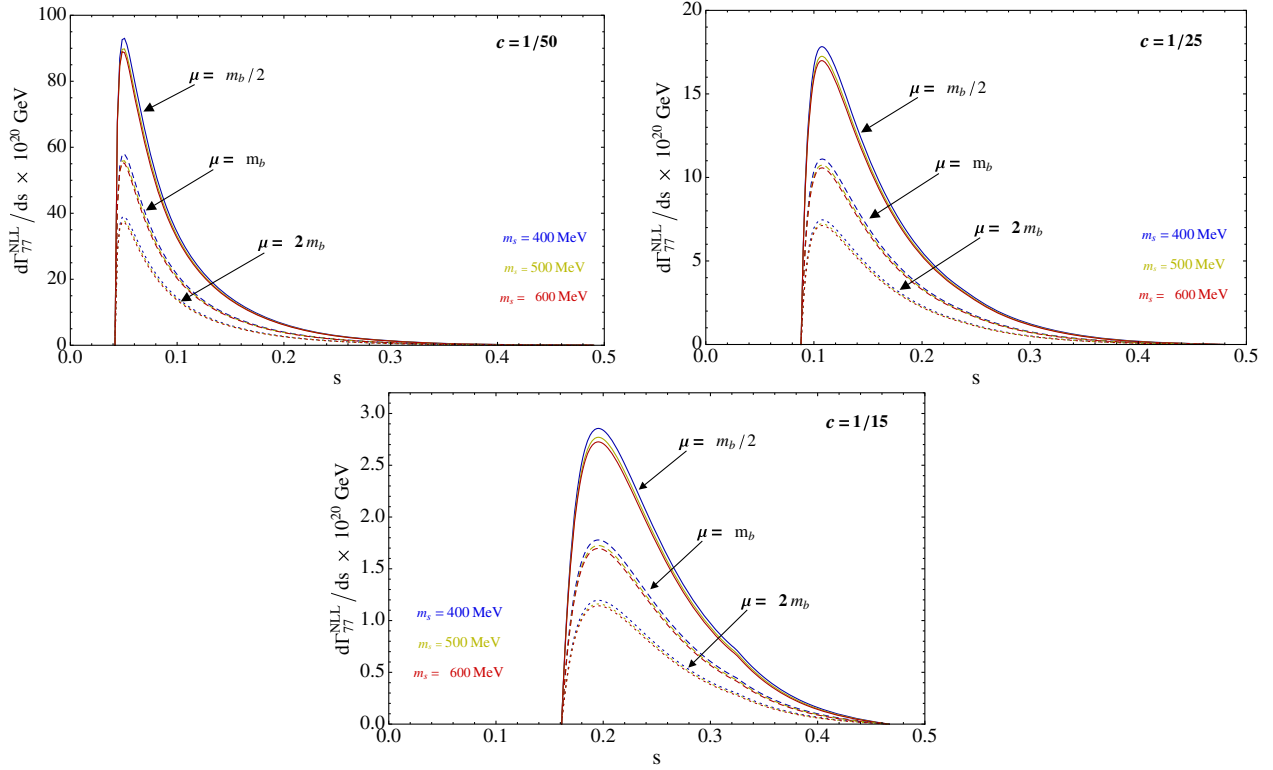


FIG. 8. $d\Gamma_{77}/ds$ at next-to-leading-order for different values of the cut-off parameter c . The first frame corresponds to $c = 1/50$, the second to $c = 1/25$ and the third to $c = 1/15$. The blue (uppermost), yellow and red (lowermost) curves in these plots describe the results when setting $m_s = 400$ MeV, $m_s = 500$ MeV and $m_s = 600$ MeV, respectively. Further, the solid (uppermost three), dashed (middle three) and dotted (lowermost three) curves in these frames define the results when choosing $\mu = m_b/2$, $\mu = m_b$ and $\mu = 2m_b$, respectively. See text for details.

In Fig. 8 we show the next-to-leading order prediction of $d\Gamma_{77}/ds$ for different values of the cut-off parameter c .

To get the branching ratio for $\bar{B} \rightarrow X_s \gamma \gamma$ as a function of the cut-off parameter c defined in Eq. (4), we integrate the double differential spectrum over the corresponding range

in s_1 and s_2 , divide by the semileptonic decay width and multiply with the measured semileptonic branching ratio. The relevant formula for the semileptonic decay width at lowest order (which is sufficient for the purpose of this paper) reads (recalling that $\hat{m}_c = m_c/m_b$)

TABLE II. Branching ratios (in units of 10^{-7}) for $\bar{B} \rightarrow X_s \gamma \gamma$. The left panel of the table corresponds to the results when choosing the kinematical cutoff parameter $c = 1/50$, the middle panel is for $c = 1/25$ and the right one for $c = 1/15$. The rows labeled as LL, LL₁, LL₂, and LL₃ stand for the improved leading-order results when setting $m_s = 0$, $m_s = 400$ MeV, $m_s = 500$ MeV, and $m_s = 600$ MeV, respectively. The rows labeled with NLL₁, NLL₂, and NLL₃ give the improved results when the calculated $O(\alpha_s)$ contributions are also included, setting $m_s = 400$ MeV, $m_s = 500$ MeV and $m_s = 600$ MeV, respectively. In this table “all” stands for the sum of all available operator contributions up-to-date at the given order.

		Branching ratios for $\bar{B} \rightarrow X_s \gamma \gamma$																	
		$c = 1/50$						$c = 1/25$						$c = 1/15$					
		$\mu = m_b/2$		$\mu = m_b$		$\mu = 2m_b$		$\mu = m_b/2$		$\mu = m_b$		$\mu = 2m_b$		$\mu = m_b/2$		$\mu = m_b$		$\mu = 2m_b$	
\mathcal{O}_7	all	\mathcal{O}_7	all	\mathcal{O}_7	all	\mathcal{O}_7	all	\mathcal{O}_7	all	\mathcal{O}_7	all	\mathcal{O}_7	all	\mathcal{O}_7	all	\mathcal{O}_7	all	\mathcal{O}_7	all
LL	0.94	0.95	0.74	0.79	0.58	0.69	0.28	0.29	0.22	0.25	0.17	0.24	0.054	0.056	0.042	0.049	0.034	0.046	
LL ₁	1.05	1.06	0.82	0.87	0.65	0.76	0.30	0.31	0.24	0.27	0.19	0.25	0.058	0.059	0.045	0.052	0.036	0.049	
LL ₂	1.11	1.12	0.87	0.92	0.69	0.79	0.31	0.32	0.25	0.28	0.19	0.26	0.059	0.061	0.046	0.054	0.037	0.051	
LL ₃	1.20	1.20	0.93	0.99	0.74	0.85	0.33	0.34	0.26	0.29	0.20	0.27	0.062	0.064	0.048	0.056	0.038	0.053	
NLL ₁	1.18	1.19	0.73	0.79	0.49	0.60	0.35	0.35	0.22	0.25	0.15	0.21	0.068	0.069	0.042	0.050	0.028	0.042	
NLL ₂	1.14	1.15	0.71	0.76	0.48	0.58	0.33	0.34	0.21	0.24	0.14	0.21	0.066	0.067	0.041	0.049	0.027	0.041	
NLL ₃	1.12	1.13	0.69	0.75	0.47	0.58	0.33	0.34	0.20	0.24	0.14	0.20	0.064	0.066	0.040	0.048	0.027	0.042	

$$\Gamma_{\text{sl}} = \frac{m_b^5 G_F^2 |V_{cb}^2|}{192\pi^3} g(\hat{m}_c), \quad (23)$$

where the phase-space factor is defined as

$$g(x) = 1 - 8x^2 + 8x^6 - x^8 - 24x^4 \log(x). \quad (24)$$

Using the input parameters in Table I, we get the branching ratios shown in Table II for different values of the cutoff parameter c .

In a previous work (see Fig. 3 of Ref. [17]), we showed that the numerical impact of the self-interference contribution of \mathcal{O}_8 to $\bar{B} \rightarrow X_s \gamma \gamma$ is minor in the full phase space and no unexpected enhancements occur, therefore it is safe to neglect this particular piece in the final numerics.

We have also investigated the relative change

$$A_{\text{rel}} = \left(\frac{\text{Br}[\bar{B} \rightarrow X_s \gamma \gamma]_{m_s \text{-exact}}^{\text{NLL}} - \text{Br}[\bar{B} \rightarrow X_s \gamma \gamma]_{m_s \rightarrow 0}^{\text{NLL}}}{\text{Br}[\bar{B} \rightarrow X_s \gamma \gamma]_{m_s \text{-exact}}^{\text{NLL}} + \text{Br}[\bar{B} \rightarrow X_s \gamma \gamma]_{m_s \rightarrow 0}^{\text{NLL}}} \right)$$

of the NLL branching ratio due to the finite m_s effects by comparing the present m_s exact result with the previous approximated result ($m_s \rightarrow 0$) of Ref. [16]. We arrive at the following conclusion: For $m_s \in [400, 600]$ MeV, A_{rel} is at most 7% when choosing the kinematical cut-off parameter c as small as $1/50$. For larger choices of c , the impact on the branching ratio from terms which contain powers of m_s becomes even less important.

VI. SUMMARY

We calculated the ($\mathcal{O}_7, \mathcal{O}_7$)-contribution to $\bar{B} \rightarrow X_s \gamma \gamma$ at $\mathcal{O}(\alpha_s)$ retaining the full dependence on the strange-quark mass m_s in our results. At this order in α_s , this requires the calculation of virtual corrections (with three body final state and a virtual gluon in the loop) and gluon bremsstrahlung corrections (tree-level contributions with four particles in the final state, one of them being massive).

We showed that for the phase-space region $(1-s_1-s_2) > c$, $(s_1-c)(s_2-c) > c$ with $c \geq 1/50$, the branching ratio for $\bar{B} \rightarrow X_s \gamma \gamma$ does not develop a sizable m_s dependence: the impact on the branching ratio is less

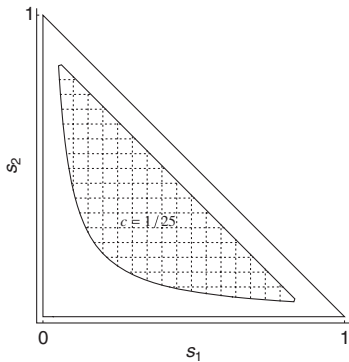


FIG. 9. Pictorial representation of the (s_1, s_2) phase-space region when choosing $c = 1/25$.

than 5% when m_s is varied between 400 and 600 MeV. Besides, we have also investigated the size of the finite strange-quark mass effects and observed that such effects are less than 7% for the same phase-space region. The observed mild sensitivity of the branching ratio on the strange-quark mass indicates that the nonperturbative effects related to the hadronic photon substructure are under control.

To give the complete results of our work, we append the Fortran program “doublediff.F” (see the corresponding paragraph after the description of Fig. 7 in Sec. V).

ACKNOWLEDGMENTS

H. M. A. is supported by the State Committee of Science of Armenia Program Grant No. 15T-1C161 and Volkswagen Stiftung Program Grant No. 86426. C. G. is supported by the Swiss National Science Foundation. A. K. acknowledges the support from the United Kingdom Science and Technology Facilities Council (STFC) under Grant No. ST/L000431/1. We thank F. Saturnino for numerically checking the ($\mathcal{O}_7, \mathcal{O}_{1,2}$) interference contributions in Eq. (9). A. K. is also thankful to Martin Gorbahn for numerous fruitful discussions.

APPENDIX A: PHASE-SPACE REGION FOR EXACT m_s CASE

In this section we give the kinematical ranges considered in this paper on the phase-space variables s_1 and s_2 in explicit form. These restricted ranges are based on Eqs. (3) and (4), leading to

$$\begin{aligned} \tilde{s}_1^- < s_1 < \tilde{s}_1^+; \quad c + \frac{c}{s_1 - c} < s_2 < 1 - s_1 - c \quad \text{with} \\ \tilde{s}_1^\pm &= (1 - c \pm \sqrt{(1-c)(1-9c)})/2, \end{aligned} \quad (\text{A1})$$

where c is the cutoff parameter satisfying $x_4 < c < 1/9$. We display in Fig. 9 the geometrical representation of Eq. (A1) when choosing $c = 1/25$.

APPENDIX B: RENORMALIZATION CONSTANTS

In this appendix, we collect the explicit expressions of the renormalization constants needed for the ultraviolet renormalization in our calculation (see Sec. IVA).

The operator \mathcal{O}_7 , as well as the b - and s -quark mass contained in this operator are renormalized in the $\overline{\text{MS}}$ scheme [58]:

$$\begin{aligned} Z_{77}^{\overline{\text{MS}}} &= 1 + \frac{4C_F \alpha_s(\mu)}{\epsilon} \frac{1}{4\pi} + \mathcal{O}(\alpha_s^2); \\ Z_{m_b}^{\overline{\text{MS}}} &= Z_{m_s}^{\overline{\text{MS}}} = 1 - \frac{3C_F \alpha_s(\mu)}{\epsilon} \frac{1}{4\pi} + \mathcal{O}(\alpha_s^2). \end{aligned} \quad (\text{B1})$$

All the remaining fields and parameters are renormalized in the on-shell scheme. The on-shell renormalization

constants for the b -quark and the s -quark masses read ($q = b$ or $q = s$)

$$Z_{m_q}^{\text{OS}} = 1 - C_F \Gamma(\epsilon) e^{\gamma\epsilon} \frac{3 - 2\epsilon}{1 - 2\epsilon} \left(\frac{\mu}{m_q}\right)^{2\epsilon} \frac{\alpha_s(\mu)}{4\pi} + O(\alpha_s^2), \quad (\text{B2})$$

while the renormalization constants for the s - and b -quark fields are given by ($q = b$ or $q = s$)

$$Z_{2q}^{\text{OS}} = 1 - C_F \Gamma(\epsilon) e^{\gamma\epsilon} \frac{3 - 2\epsilon}{1 - 2\epsilon} \left(\frac{\mu}{m_q}\right)^{2\epsilon} \frac{\alpha_s(\mu)}{4\pi} + O(\alpha_s^2). \quad (\text{B3})$$

-
- [1] M. Misiak, H. Asatrian, R. Boughezal, M. Czakon, T. Ewerth *et al.*, *Phys. Rev. Lett.* **114**, 221801 (2015).
- [2] F. Borzumati and C. Greub, *Phys. Rev. D* **58**, 074004 (1998).
- [3] F. Borzumati and C. Greub, *Phys. Rev. D* **59**, 057501 (1999).
- [4] M. Ciuchini, G. Degrassi, P. Gambino, and G. F. Giudice, *Nucl. Phys.* **B527**, 21 (1998).
- [5] T. Hermann, M. Misiak, and M. Steinhauser, *J. High Energy Phys.* **11** (2012) 036.
- [6] I. Heredia de la Cruz, *J. Phys. Conf. Ser.* **761**, 012017 (2016).
- [7] T. Aushev *et al.*, [arXiv:1002.5012](https://arxiv.org/abs/1002.5012).
- [8] M. Misiak, H. Asatrian, K. Bieri, M. Czakon, A. Czarnecki *et al.*, *Phys. Rev. Lett.* **98**, 022002 (2007).
- [9] T. Hurth and M. Nakao, *Annu. Rev. Nucl. Part. Sci.* **60**, 645 (2010).
- [10] A. J. Buras, [arXiv:1102.5650](https://arxiv.org/abs/1102.5650).
- [11] H. Simma and D. Wyler, *Nucl. Phys.* **B344**, 283 (1990).
- [12] L. Reina, G. Ricciardi, and A. Soni, *Phys. Lett. B* **396**, 231 (1997).
- [13] L. Reina, G. Ricciardi, and A. Soni, *Phys. Rev. D* **56**, 5805 (1997).
- [14] J.-j. Cao, Z.-j. Xiao, and G.-r. Lu, *Phys. Rev. D* **64**, 014012 (2001).
- [15] H. Asatrian, C. Greub, A. Kokulu, and A. Yeghiazaryan, *Phys. Rev. D* **85**, 014020 (2012).
- [16] H. M. Asatrian and C. Greub, *Phys. Rev. D* **89**, 094028 (2014).
- [17] H. M. Asatrian, C. Greub, and A. Kokulu, *Phys. Rev. D* **93**, 014037 (2016).
- [18] A. Gemintern, S. Bar-Shalom, and G. Eilam, *Phys. Rev. D* **70**, 035008 (2004).
- [19] C.-H. V. Chang, G.-L. Lin, and Y.-P. Yao, *Phys. Lett. B* **415**, 395 (1997).
- [20] G. Hiller and A. S. Safir, *J. High Energy Phys.* **02** (2005) 011.
- [21] A. Y. Ignatiev, G. C. Joshi, and B. McKellar, *Int. J. Mod. Phys. A* **20**, 4079 (2005).
- [22] G. Hiller and E. Iltan, *Phys. Lett. B* **409**, 425 (1997).
- [23] S. W. Bosch and G. Buchalla, *J. High Energy Phys.* **08** (2002) 054.
- [24] S. W. Bosch, [arXiv:hep-ph/0208203](https://arxiv.org/abs/hep-ph/0208203).
- [25] G. Hiller and A. S. Safir, *Proc. Sci.*, HEP2005 (2006) 277.
- [26] G.-L. Lin, J. Liu, and Y.-P. Yao, *Phys. Rev. Lett.* **64**, 1498 (1990).
- [27] S. Herrlich and J. Kalinowski, *Nucl. Phys.* **B381**, 501 (1992).
- [28] S. Choudhury, G. C. Joshi, N. Mahajan, and B. McKellar, *Phys. Rev. D* **67**, 074016 (2003).
- [29] T. Aliev, G. Hiller, and E. Iltan, *Nucl. Phys.* **B515**, 321 (1998).
- [30] S. Bertolini and J. Matias, *Phys. Rev. D* **57**, 4197 (1998).
- [31] I. I. Bigi, G. Chiladze, G. Devidze, C. Hanhart, A. Lipartelian *et al.*, *GESJ Phys.* **2006N1**, 57 (2006).
- [32] G. Devidze and G. Jibuti, [arXiv:hep-ph/9810345](https://arxiv.org/abs/hep-ph/9810345).
- [33] T. Aliev and G. Turan, *Phys. Rev. D* **48**, 1176 (1993).
- [34] Z.-j. Xiao, C.-D. Lu, and W.-j. Huo, *Phys. Rev. D* **67**, 094021 (2003).
- [35] W.-j. Huo, C.-D. Lu, and Z.-j. Xiao, [arXiv:hep-ph/0302177](https://arxiv.org/abs/hep-ph/0302177).
- [36] H. Chen and W. Huo, [arXiv:1101.4660](https://arxiv.org/abs/1101.4660).
- [37] X.-M. Qin, W.-J. Huo, and X.-F. Yang, *Chin. Phys. C* **33**, 252 (2009).
- [38] K. G. Chetyrkin, M. Misiak, and M. Munz, *Phys. Lett. B* **400**, 206 (1997).
- [39] M. Gorbahn and U. Haisch, *Nucl. Phys.* **B713**, 291 (2005).
- [40] M. Gorbahn, U. Haisch, and M. Misiak, *Phys. Rev. Lett.* **95**, 102004 (2005).
- [41] M. Czakon, U. Haisch, and M. Misiak, *J. High Energy Phys.* **03** (2007) 008.
- [42] C. Bobeth and A. Kokulu (to be published).
- [43] H. M. Asatrian, A. Hovhannisyan, and A. Yeghiazaryan, *Phys. Rev. D* **86**, 114023 (2012).
- [44] M. Kaminski, M. Misiak, and M. Poradzinski, *Phys. Rev. D* **86**, 094004 (2012).
- [45] H. M. Asatrian and C. Greub, *Phys. Rev. D* **88**, 074014 (2013).
- [46] S. Frixione, *Phys. Lett. B* **429**, 369 (1998).
- [47] S. Laporta, *Int. J. Mod. Phys. A* **15**, 5087 (2000).
- [48] F. Tkachov, *Phys. Lett.* **100B**, 65 (1981).
- [49] K. Chetyrkin and F. Tkachov, *Nucl. Phys.* **B192**, 159 (1981).
- [50] R. Mertig, M. Bohm, and A. Denner, *Comput. Phys. Commun.* **64**, 345 (1991).
- [51] V. Shtabovenko, R. Mertig, and F. Orellana, *Comput. Phys. Commun.* **207**, 432 (2016).

- [52] T. Hahn and M. Perez-Victoria, *Comput. Phys. Commun.* **118**, 153 (1999).
- [53] G. J. van Oldenborgh and J. A. M. Vermaseren, *Z. Phys. C* **46**, 425 (1990).
- [54] S. Borowka, G. Heinrich, S. P. Jones, M. Kerner, J. Schlenk, and T. Zirke, *Comput. Phys. Commun.* **196**, 470 (2015).
- [55] G.'t Hooft and M. J. G. Veltman, *Nucl. Phys.* **B153**, 365 (1979).
- [56] A. Denner, *Fortschr. Phys.* **41**, 307 (1993).
- [57] T. Hahn, *Comput. Phys. Commun.* **168**, 78 (2005).
- [58] M. Misiak and M. Munz, *Phys. Lett. B* **344**, 308 (1995).